The 15th International Symposium on Magnetic Bearings, August 3-6, 2016, Mojiko Hotel, Kitakyushu, Japan

ISMB15

Stability improvement of passively stabilized degrees of freedom in magnetically levitated systems

Hubert MITTERHOFER* and Gerald JUNGMAYR**

*Linz Center of Mechatronics

Altenbergerstrasse 69, 4040 Linz, Austria

E-mail: hubert.mitterhofer@lcm.at

**Institute of Electrical Drives and Power Electronics, Johannes Kepler University Linz

Altenbergerstrasse 69, 4040 Linz, Austria

Abstract

The passive degrees of freedom of magnetically levitated devices are prone to external disturbance forces and torques as there is no possibility to adapt the bearing stiffness or to introduce damping actively. In the case of bearingless disk drives, this concerns the axial and tilt deflections. A novel stabilization coil presented in this work helps to stabilize the tilt deflections. After the introduction of the electrodynamic working principle, the measurement results conducted at a high speed bearingless disk drive prototype are presented. To the knowledge of the authors, this work represents the first publication on such a stabilization device.

Keywords : Tilt Stabilization, Electrodynamic Bearing, Disk Drive, Gyroscopic Motion, Passive Damping

1. Introduction

A body disposes of six motional degrees of freedom (DOFs) of which, for the case of rotational drives, five need to be stabilized. Many different approaches are known for stabilizing a rotor by using magnetic levitation – ranging from fully active arrangements to combinations of passive and active stabilization.

In bearingless drives which offer a significant reduction of mechanical complexity by integrating an active magnetic bearing and the electrical drive, highly compact designs are possible. The mechanically most compact one, offering the most significant reduction in the part count of a drive is a bearingless disk drive with combined windings as presented e.g. in (Steinert et al., 2014) or (Mitterhofer et al., 2014). This drive type consists of only one motor/bearing plane where, with one common set of rotor magnets, one set of stator windings and one common back iron, all necessary stabilization forces and torques including the drive torque are generated.

This compactness comes at the price that the axial and tilt DOFs are only passively stabilized without any influence of the control circuit as shown in Fig. 1. This work presents a very simple method on how to stabilize the tilt DOF by inserting a coil into the stator. To the knowledge of the author, this is a novel approach for stabilizing the tilt DOF, especially at high speed operation, without giving up the compactness advantage.

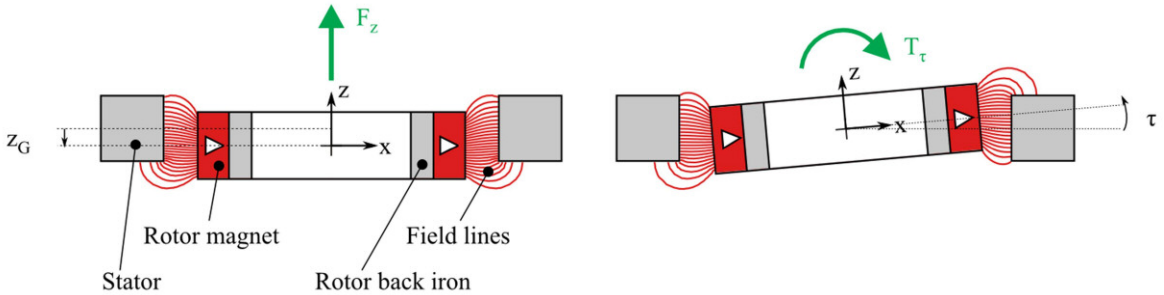

Fig. 1 Passive stabilization in a bearingless disk drive with axial deflection z_G with restoring force F_z (left) and tilt deflection τ with restoring torque T_τ (right).

2. Problem statement due to passively stabilized DOFs

While the stiffness of actively stabilized DOFs can be adapted to the current load case, the stiffness value of a passively stabilized DOF is fixed. Additionally, many typical applications for magnetic levitation technology demand large air gaps which typically reduce the axial and tilt stiffness values.
More stringent than the low stiffness, the inability to add damping via an active control circuit poses the problem that resonance phenomena may lead to system failure when the passive DOF motion is stimulated by an internal or external disturbance force or torque. The critical axial resonance frequency of a bearingless disk drive is given as

$$\Omega_{c,z} = \sqrt{\frac{c_z}{m_R}} \tag{1}$$

where c_z and m_R denote the axial stiffness and rotor mass, respectively. The corresponding critical tilt resonance for standstill and isentropic stiffness, e.g. in a four-pole magnetic rotor is

$$\Omega_{c,\tau} = \sqrt{\frac{\bar{c}_\tau}{I_d}} \tag{2}$$

where $\bar{c}_\tau$ stands for the mean value of the tilt stiffness and I_d gives the diametric moment of inertia. For the rotating situation, Eq.(2) splits into two frequencies for forward and backward mode (index f and b) according to

$$\Omega_{c,\tau_{f,b}} = \frac{I_p\Omega \pm \sqrt{(I_p\Omega)^2 + 4\bar{c}_\tau I_d}}{2I_d}, \tag{3}$$

additionally holding the polar moment of inertia I_p. When a two-pole rotor is considered, the ratio of polar to diametric moment of inertia ξ and the variation ratio of the tilt stiffness $\hat{c}_\tau$ are necessary to give the enlarged definition of the critical tilt resonance frequencies as

$$\Omega_{c,\bar{\tau}_{f,b}} = \Omega \pm \sqrt{\frac{\bar{c}_\tau}{I_d} + \Omega^2\left(1 + \frac{1}{2}\xi^2 - \xi\right) \mp \sqrt{\Omega^4\xi^2\left(1 - \frac{1}{2}\xi\right)^2 + \frac{\bar{c}_\tau}{I_d}\Omega^2(2-\xi)^2 + \frac{\bar{c}_\tau^2}{I_d^2}\hat{c}_\tau^2}} \tag{4}$$

which show that the tilt problem is not limited to a quasi-static deflection but that it is coupled with the rotor speed Ω. A more detailed analysis of the rotordynamic behavior of a magnetically levitated disk can be found in (Grabner, 2007). As clearly visible in Fig. 2, the resonance frequencies of Eq.(3) and Eq.(4), respectively, both exhibit a forward whirl and a backward whirl. The depicted curves assume $1 < \xi < 2$ and $\hat{c}_\tau = 0.5$.

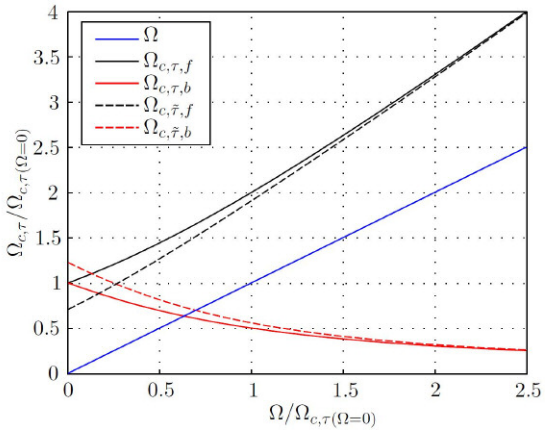

Fig. 2 Critical tilt stiffness curves over rotational speed Ω for isotropic (solid lines) and anisotropic (dashed lines) tilt stiffness, both normalized to the static critical tilt resonance frequency

Regardless of the stiffness values, Fig. 2 clearly shows that the backward whirl motion is sensitive to very low excitation frequencies as the rotational speed increases. Unfortunately, the passive tilt stabilization of a bearingless disk drive usually disposes of very little inherent damping, which means that this backward whirl movement can easily unfold if excited. The nearly undamped deflections of the whirling rotor can cause a rotor-stator contact. This reduces the lifetime of the touchdown bearings at high rotational speeds.

3. State of the art for additional damping

Only few methods can be considered for adding contact-free damping to a passively stabilized DOF. One of them is to provide an appropriate support of the stator, e.g. in form of visco-elastic dampers. The authors of (Marth et al. 2010) have demonstrated the effectiveness of this method for suppressing vibrations of a magnetically levitated shaft. However, while the shaft translations in that work had notable amplitudes and frequencies, the tilt movement in the present drive can be very small in amplitude and low in frequency. Also, a visco-elastic stator support is very demanding concerning material life time, precision and may not be suitable in many applications.

A second source of damping can be a medium, surrounding the rotor, with higher viscosity than air. This is relevant for most magnetically levitated pump applications as e.g. in blood pumps (Nussbaumer et al. 2011), (Raggl et al. 2009) or blenders for the pharmaceutical industry (Warberger et al. 2012) which operate in liquids. However, this sort of damping can usually not be added randomly - dependent on the application it is either present or it is not.

Additionally, electrodynamic dampers can be applied. The principle of electrodynamic dampers appeared in the 1970's, usually connected to the support of railway vehicles (Atherton and Eastham 1973) and surfaced again later, now focused on the stabilization of rotors (Davey et al. 2005), (Detoni et al. 2012), (Kluyskens and Dehez 2013). Two extensive works (Lembke 2005) and (Impinna 2010) describe different forms and design criteria for such electrodynamic bearings and dampers. They mostly focus on elements with homopolar permanent magnetic fields and rotor-bound conductors where stabilization currents are induced. Additional works of Davey and Filatov (Davey et al. 1995, Davey et al. 2005, and Filatov and Maslen 2001) propose so-called *Null flux bearings* which dispose of coils that only experience a net linked flux if a rotor carrying a heteropolar magnetic field is radially or axially displaced from its central position. Other than in the described works, the tilt stabilization coil presented in this chapter does not require additional magnetic means.

4. Principle of the proposed tilt stabilization coil

The proposed stabilization uses the rotating diametrical permanent magnet field of the present bearingless disk rotor and only requires an additional short-circuited winding in the stator, placed as shown in Fig. 3. In the centered and non-tilted rotor position, the newly introduced tilt stabilization coil (TSC) does not experience an induced voltage. The permanent magnet flux splits equally to the upper and lower half of the stator iron. When the rotor is tilted, the fluxes at the magnet poles are no longer equally distributed but are more concentrated in the upper or lower stator half, respectively. This is shown in Fig. 4.

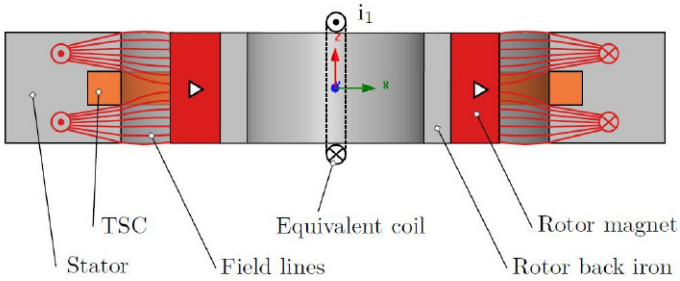

Fig. 3 Bearingless disk drive with an additional stabilization coil (TSC) and an equivalent coil, energized by i_1 for modelling the permanent magnet.

The largest share of the magnetic flux still leaves the stator core in the same half that it has entered (red flux lines). However, a part of the flux (green flux lines) crosses from one half to the other - leaving the magnet, crossing the air gap, entering the stator (e.g. in the lower half of the stator), flowing through the stator to the opposite side, leaving the stator (e.g.: from the upper stator half), again crossing the air gap and entering back into the magnet. This means that there is a net flux closing through the TSC.

The described paths change when the non-rotating rotor tilts back and forth about one axis but the frequency of this movement is relatively low, causing only low induced voltage and thus, low values of the short-circuit current i_2. However, as the rotor rotates with a quasi-statically tilted axis of rotation, the pole orientation changes and so does the direction of the flux through the TSC. The quasi-static consideration seems legitimate when the rotational frequency is significantly higher than the tilting frequency. The mentioned flux change induces a voltage which will drive the

current i_2 through the TSC. Due to the high frequency of rotation compared to the case of pure tilting movement, the induced voltage and the current i_2 are significantly larger in this case. The resulting effect on the precession movement was confirmed by introducing a TSC, similar to the one shown here, into an existing disk drive.

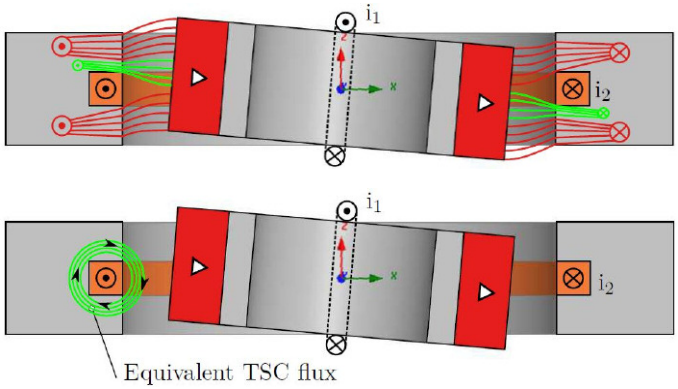

Fig. 4 The tilted rotor provokes unequal flux distribution (top) leading to a net equivalent flux through the TSC (bottom)

5. Equation of motion

For finding a valid equation of motion, we assume an initial situation of a radially centered rotor which is tilted about the stator-fixed x- and y-axis specified in Fig. 5. The variables $\alpha(t), \beta(t), \varphi(t)$, and $i_2(t)$ are time-dependent. For the sake of readability, they will be written as α, β, φ, and i_2.

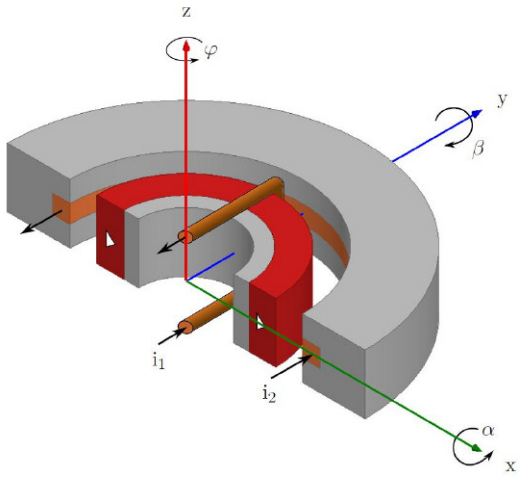

Fig. 5 Stator coordinate system, relevant angles, and current variables for the stabilization model. The magnetic field of the rotor magnet can also be generated by an imagined coil with a constant equivalent current i_1. The TSC, conducting i_2 is embedded in the actual stator of the prototype.

Generally, the magnetic co-energy $W_{m,co}$ of a conservative, electromagnetic system with one coil is

$$W_{m,co} = \int \Psi di \tag{5}$$

where Ψ is the linked flux due to the current i. For the present case of a two coil system, Eq.(5) evaluates to

$$W_{m,co} = \frac{1}{2}L_{11}i_1^2 + L_{12}i_1i_2 + \frac{1}{2}L_{22}i_2^2 \tag{6}$$

where the inductances L_{11} and L_{12} depend on the angles α, β and φ and where L_{22} is constant. The current i_1 is also constant while i_2, circulating in the TSC, is also coupled with the angles α, β and φ. Differentiating Eq.(6) with respect to the tilt angles yields the resulting tilt torques

$$T_\alpha = \frac{\partial W_{m,co}}{\partial \alpha} = \frac{\partial}{\partial \alpha}\left(\frac{L_{11}i_1^2}{2} + L_{12}i_1i_2\right) \quad \text{and} \quad T_\beta = \frac{\partial W_{m,co}}{\partial \beta} = \frac{\partial}{\partial \beta}\left(\frac{L_{11}i_1^2}{2} + L_{12}i_1i_2\right) \tag{7}$$

which can be decomposed into the coupling torque terms

$$T_{TSC,\alpha} = \frac{\partial L_{12}i_1i_2}{\partial \alpha} \quad \text{and} \quad T_{TSC,\beta} = \frac{\partial L_{12}i_1i_2}{\partial \beta} \tag{8}$$

due to the newly introduced TSC and into the reluctance terms

$$T_{\tau,\alpha} = \frac{1}{2}\frac{\partial L_{11} i_1^2}{\partial \alpha} = \bar{c}_\tau(1 - \hat{c}_\tau \cos(2\Omega t))\alpha + \bar{c}_\tau \hat{c}_\tau \sin(2\Omega t)\beta \quad \text{and}$$

$$T_{\tau,\beta} = \frac{1}{2}\frac{\partial L_{11} i_1^2}{\partial \beta} = \bar{c}_\tau \hat{c}_\tau \sin(2\Omega t)\,\alpha + \bar{c}_\tau(1 + \hat{c}_\tau \cos(2\Omega t))\beta \tag{9}$$

according to the formulation of stiffness anisotropy of a two-pole rotor found in literature, e.g. (Grabner 2007).

a. Coupling term

The component $\hat{L}_{12}$ is the peak coupling inductance value between the TSC and the equivalent coil when the two are collocated in the same plane. The peak value, however, only appears when the magnet is tilted upright, with the vector of magnetization pointing up or downwards. Generally, L_{12} can be described as

$$L_{12} = -\hat{L}_{12} \sin(\beta) \cos(\Omega t) + \hat{L}_{12} \sin(\alpha) \cos(\Omega t) \tag{10}$$

where α and β are time dependent. These tilt angles are relatively small in amplitude and change slowly compared to the rotational angle Ωt. This means that linearization, yielding

$$L_{12} = -\hat{L}_{12}\beta \cos(\Omega t) + \hat{L}_{12}\alpha \cos(\Omega t) \tag{11}$$

is possible for small deviations. Substituting into Eq.(8), the coupling torque components can be written as

$$T_{TSC,\alpha} = \frac{\partial}{\partial \alpha}\left[\hat{L}_{12}(\alpha \cos(\Omega t) - \beta \cos(\Omega t)) i_1 i_2\right] \quad \text{and} \quad T_{TSC,\beta} = \frac{\partial}{\partial \beta}\left[\hat{L}_{12}(\alpha \cos(\Omega t) - \beta \cos(\Omega t)) i_1 i_2\right] \tag{12}$$

showing the influence of the tilt angles but also of the unknown TSC-current i_2.

b. TSC current

The voltage equation for the short-circuited coil

$$V_2 = i_2 R_2 + \frac{d\Psi_2}{dt} = 0 \tag{13}$$

can be combined with the linear relationship between the coil sum flux value Ψ_2 and the coupling and self-inductance

$$\Psi_2 = L_{12} i_1 + L_{22} i_2. \tag{14}$$

After using Eq.(11) and deriving Ψ_2 with respect to time, we obtain an additional differential equation

$$L_{22}\frac{di_2}{dt} + i_2 R_2 + \hat{L}_{12} i_1\left(\alpha \cos(\Omega t)\Omega + \dot{\alpha} \cos(\Omega t) + \beta \cos(\Omega t)\beta - \dot{\beta} \cos(\Omega t)\right) = 0 \tag{15}$$

for the TSC current which can now be coupled with the differential equations for the tilt angles.

c. Nonlinear differential equation

The TSC behavior modeled in Eq.(9), Eq.(12), and Eq.(15) can be combined with a standard Jeffcott rotor model. Selecting the state vector as $\boldsymbol{q} = \begin{bmatrix} \alpha \\ \beta \\ i_2 \end{bmatrix}$ allows coupling the electric and the mechanic system as

$$\boldsymbol{I} \cdot \ddot{\boldsymbol{q}} + (\boldsymbol{G} + \boldsymbol{D}) \cdot \dot{\boldsymbol{q}} + \boldsymbol{C} \cdot \boldsymbol{q} = \boldsymbol{0} \tag{16}$$

with the inertia matrix, gyroscopic matrix, damping matrix and stiffness matrix populated as follows:

$$\boldsymbol{I} = \begin{bmatrix} I_d & 0 & 0 \\ 0 & I_d & 0 \\ 0 & 0 & 0 \end{bmatrix}, \quad \boldsymbol{G} = \begin{bmatrix} 0 & I_p\Omega & 0 \\ -I_p\Omega & 0 & 0 \\ 0 & 0 & 0 \end{bmatrix}, \quad \boldsymbol{D} = \begin{bmatrix} D_\tau & 0 & 0 \\ 0 & D_\tau & 0 \\ \hat{L}_{12} i_1 \sin(\Omega t) & -\hat{L}_{12} i_1 \cos(\Omega t) & L_{22} \end{bmatrix},$$

$$\boldsymbol{C} = \begin{bmatrix} \bar{c}_\tau(1 - \hat{c}_\tau \cos(2\Omega t)) & \bar{c}_\tau \hat{c}_\tau \sin(2\Omega t) & -\hat{L}_{12} i_1 \sin(\Omega t) \\ \bar{c}_\tau \hat{c}_\tau \sin(2\Omega t) & \bar{c}_\tau(1 + \hat{c}_\tau \cos(2\Omega t)) & \hat{L}_{12} i_1 \cos(\Omega t) \\ \hat{L}_{12} i_1 \cos(\Omega t)\, \Omega & \hat{L}_{12} i_1 \sin(\Omega t)\, \Omega & R_2 \end{bmatrix}.$$

d. Numerical simulation

In order to analyze the behavior of the complete differential equation system as given in Eq.(16), a numerical simulation was conducted. The model was implemented and simulated in Matlab/Simulink®. Most of the key parameters listed in Table 1 were obtained directly or indirectly from the real prototype. The damping parameter D_τ and the coupling inductance peak value $\hat{L}_{12}$ were identified from the measurements shown in Fig. 8. The tilt stiffness coefficients were obtained by finite element simulation and corrected via comparison between the numerical simulation of Eq.(16) and the measurement results in Fig. 8. Only the equivalent current i_1 was determined analytically.

Table 1 Parameters of drive prototype also used in simulation

Parameter	Value		Parameter	Value
I_d	3.75e-6 kg m²		$\hat{L}_{12}$	0.44 µH
I_p	6.4e-6 kg m²		L_{22}	180 µH
D_τ	8e-4 Nm s		R_2	0.98 Ω
$\bar{c}_\tau$	0.35 Nm/rad		i_1	20200 A
$\hat{c}_\tau$	0.65			

The numerical model was evaluated in order to present the difference between an ideally undamped system without TSC, a system with damping (due to eddy currents and air drag, parameter identified at real prototype) but also without TSC, and a system with the same damping parameter and TSC. The results in Fig. 6 allow several conclusions:

- At low rotational speeds, the damping of the system is effective for stabilizing the oscillation of the tilt angle. The TSC shows no notable effect at this point. It needs to be mentioned that the shown deflections are higher as the tolerable deflections in a real drive.
- At a speed of 50krpm, the occurring angle deflection amplitudes are reduced due to the gyroscopic behavior of a rotating disk and, as predicted in Fig. 2, the backward whirl frequencies are lowered. The damping does effectively remove the high frequency forward whirl, visible in the fact that the thick black line in Fig. 6 is reduced to a thin blue line. The slow backward whirl movement, however, is not damped sufficiently. The simulation including a TSC predicts swift stabilization of all tilt movements.

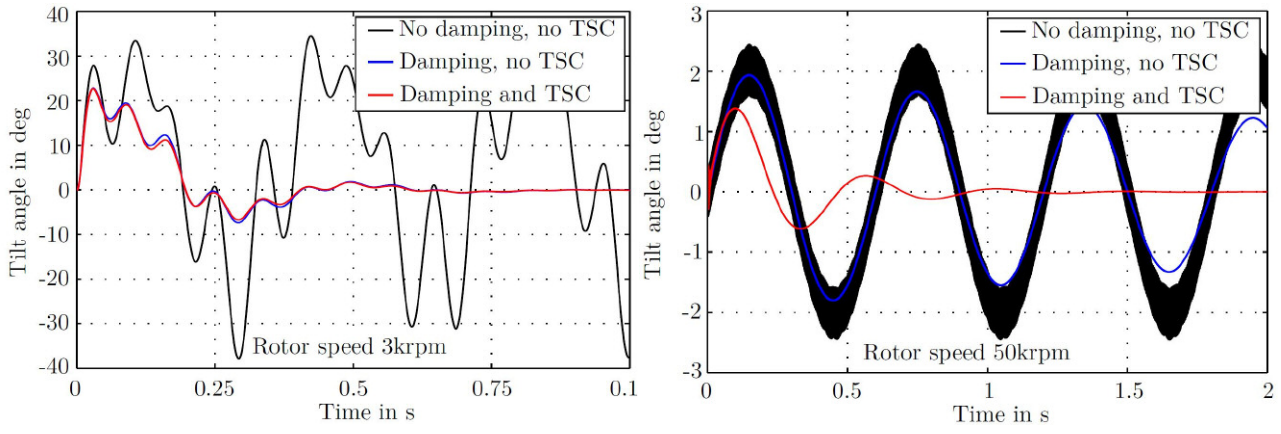

Fig. 6 Comparison of models with and without damping and TSC, respectively, at 3krpm (left) and 50krpm (right).

6. Measurement results

In order to verify the proposed numerical model, measurements were conducted at a prototype holding a TSC. As stated above, the parameters of the numerical model were measured or identified from this prototype. In order to test the behavior of the drive with this new feature, a torque impulse has to act on the spinning rotor. This is, however, a difficult task because an impulse hammer cannot be used on a spinning rotor. Therefore, the following measuring procedure was defined for measuring the TSC effect with a test rig shown in Fig. 7.

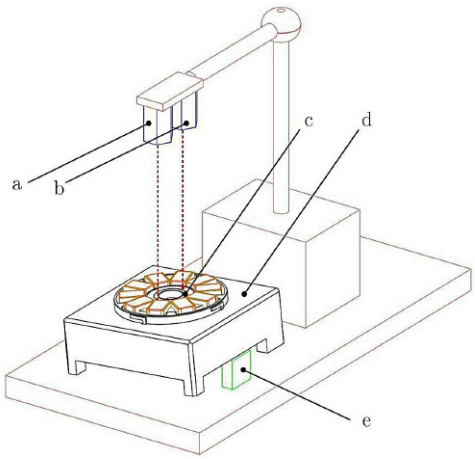

- Acceleration of the rotor to target speed
- Adjustment of optical distance sensors (a) and (b) in order to measure the axial deflections z_a and z_b at two opposite positions of the rotor (c) at a known radial distance r_{sens} from the rotor center
- Slow tilting of the entire drive unit (d) to allow the placement of a defined spacer (e) on a defined position under the drive housing
- Triggering of measurement by sharply pulling spacer out from under the drive unit (d)
- Evaluation of the tilt angle according to

$$\alpha = \tan\left(\frac{z_a - z_b}{r_{sens}}\right)$$

Fig. 7 Tilt measurement apparatus with two optical sensors (a) and (b), measuring the axial deflection of the spinning rotor (c) when the drive (d) is tilted by removing a spacer (e).

Figure 8 compares the tilt angle of the measurement with the simulation of the proposed model at a rotor speed of 25krpm and 50krpm, respectively.

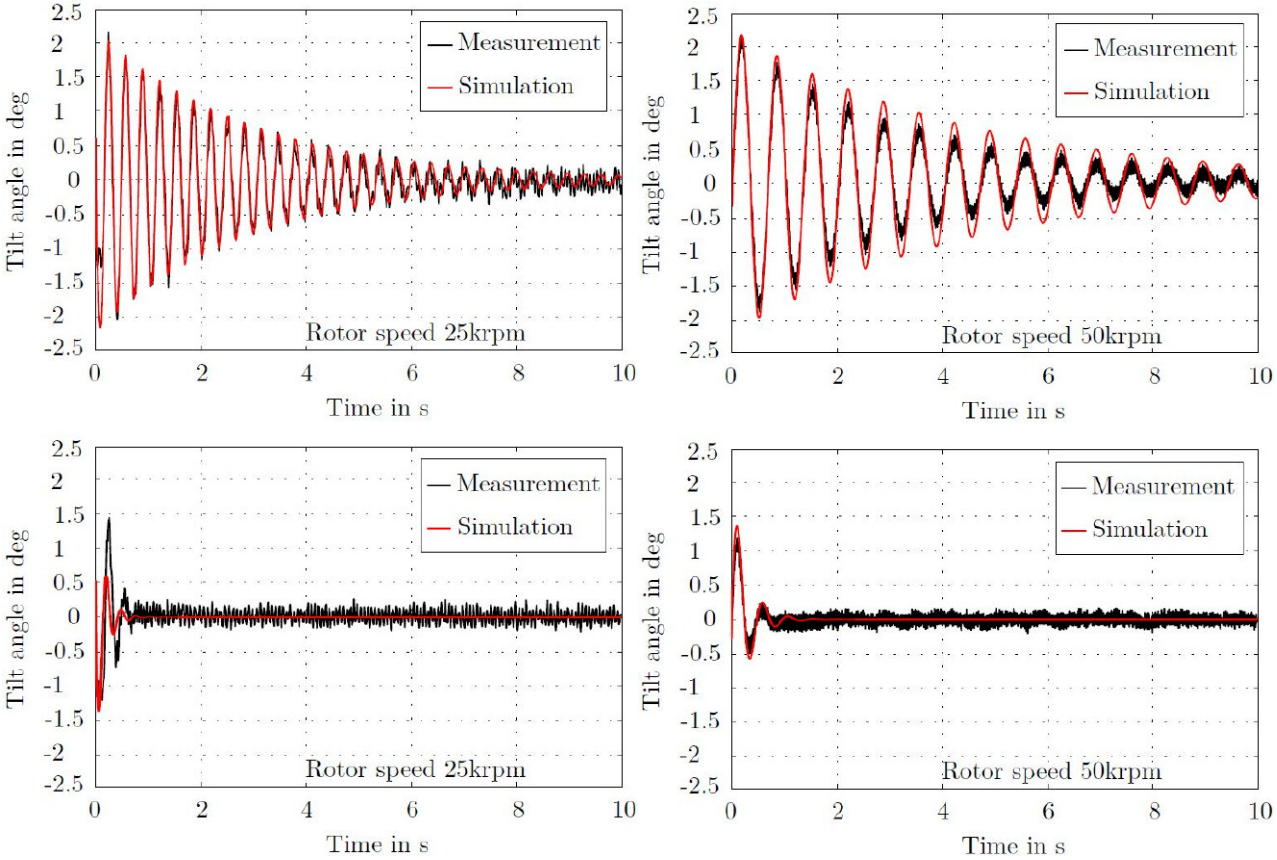

Fig. 8 Comparison of measured and simulated tilt angle at 25kprm (left) and 50krpm (right) with deactivated (top) and activated TSC (bottom)

7. Conclusions and outlook

The findings of this work which are subject to a pending patent application lead to the following conclusions:

- The effect of the activated (short circuited) TSC in the simulations and measurements shown in Fig. 8 is tremendous compared to the deactivated (opened) TSC where only the surrounding air and the speed-dependent eddy currents in the stator core provide damping.
- There is very good correlation between the measurement and the simulation when the actual external damping and the passive tilt stiffness have been identified.
- The TSC provides mechanically simple, robust, and highly compact passive tilt stabilization. While presented using the example of a disk shaped bearingless drive, the principle is applicable to many other drives.

Depending on the rotor-stator-combination that the TSC shall be applied to, several different winding forms, all causing the identical effects, can be found. Further works will present some basic characteristics common to these forms as well as the active bearing functions which can be realized with them.

8. Acknowledgement

This work was conducted within the COMET-K2 program of the Linz Center of Mechatronics (LCM), and was funded by the Austrian federal government and the federal state of Upper Austria. The authors thank all involved partners for their support.

References

Atherton, D. and Eastham, A.R., "Flat guidance schemes for magnetically levitated highspeed guided ground transport," Journal of Applied Physics, vol. 45, 1973.

Davey, K., Morris, T., Shaaf, J., and Rote, D.,"Calculation of motion induced eddy current forces in null flux coils," IEEE Transactions on Magnetics, vol. 31, no. 6, 1995.

Davey, K., Filatov, A., and Thompson, R., "Design and analysis of passive homopolar null flux bearings," IEEE Transactions on Magnetics, vol. 41, no. 3, pp. 1169–1175, 2005.

Detoni, J. G., Impinna, F., Amati, N., and Tonoli, A., "Rotordynamic stabilization of rotors on electrodynamic bearings," INTECH Open, vol. Advances in Vibration Engineering and Structural Dynamics, pp. 51–66, 2012.

Filatov, A., and Maslen E., "Passive magnetic bearing for flywheel energy storage systems," IEEE Transactions on Magnetics, vol. 37, no. 6, pp. 3913–3924, 2001.

Grabner, H., "Dynamik und Ansteuerkonzepte Lagerloser Drehfeld- Scheibenlaeufermotoren in Radialer Bauform," Ph.D. dissertation, JKU, 2007.

Impinna, F., "Electrodynamic bearings," Ph.D. dissertation, Politecnico di Torino, 2010.

Kluyskens, V. and Dehez, B., "Dynamical electromechanical model for magnetic bearings subject to eddy currents," IEEE Transactions on Magnetics, vol. 49, pp. 1444– 1453, 2013.

Lembke, T., "Design and analysis of a novel low loss homopolar electrodynamic bearing," Ph.D. dissertation, KTH Stockholm, 2005.

Marth, E., Jungmayr, G., and Amrhein, W., "Influence of viscoelastic elements on magnetically passive stabilized degrees of freedom," Proc. 13th International Symposium on Magnetic Bearings, 2010.

Mitterhofer, H., Gruber, W., and Amrhein, W., "On the high speed capacity of bearingless drives," IEEE Transactions on Industrial Electronics, vol. 61, no. 6, pp. 3119– 3126, 2014.

Nussbaumer, T., Karutz, P., Zuercher, F., and Kolar, J., "Magnetically levitated slice motors—an overview," IEEE Transactions on Industry Applications, vol. 47, no. 2, pp. 754–766, 2011.

Raggl, K., Warberger, B., Nussbaumer, T., Burger, S., and Kolar, J. W., "Robust angle sensorless control of a PMSM bearingless pump," IEEE Transactions on Industrial Electronics, vol. 56, pp. 2076–2085, 2009.

Steinert, D. and Nussbaumer, T. and Kolar, J., „Slotless bearingless disk drive for high-speed and high-purity applications", IEEE Transactions on Industrial Electronics, 61, 2014.

Warberger, B., Kaelin, R., Nussbaumer, T., and Kolar, J., "50Nm / 2500W bearingless motor for high-purity pharmaceutical mixing," IEEE Transactions on Industrial Electronics, vol. 59, pp. 2236–2247, 2012.